Next Materials 12 (2026) 102399

Contents lists available at ScienceDirect

Next Materials

journal homepage: www.sciencedirect.com/journal/next-materials

Research article

Electrochemical tracking of sulphadiazine with a SnO_2-PANI functionalized carbon paste electrode

Aishwarya S. Sajjan, Swastika N. Das *, Kailash S. Chadchan, Ramesh S. Malladi

Department of Chemistry, BLDEA's V. P. Dr. P. G. Halakatti College of Engineering and Technology, (affiliated to Visvesvaraya Technological University, Belagavi), Vijayapur, Karnataka 586103, India

ARTICLE INFO

Keywords:
Sulphadiazine
Cyclic voltammetry
Differential pulse voltammetry
SnO_2 nanoparticles
PANI
Carbon paste electrode

ABSTRACT

Sulphadiazine (SDZINE) is widely used in clinical and veterinary practice, and its residues in food and environmental matrices require simple and cost-effective detection approaches. In this study, a SnO_2-polyaniline nanocomposite-modified carbon paste electrode (SnO_2–PANI/MCPE) was fabricated for the electrochemical detection of SDZINE. SnO_2 and PANI were synthesised and incorporated into a modified carbon paste electrode, and the material was characterised using SEM-EDX, XRD, and FTIR. Electrochemical performance was evaluated using cyclic voltammetry and differential pulse voltammetry in 0.2 M phosphate buffer solution at pH 7.4. The SnO_2-PANI/MCPE showed enhanced anodic response compared with the bare carbon paste electrode (BCPE) and individually modified electrodes, indicating improved electrocatalytic activity toward SDZINE oxidation. Scan-rate studies suggested a mixed diffusion-adsorption controlled process with significant adsorption contribution, while pH studies supported proton involvement in the oxidation process. Under optimised conditions, the sensor exhibited a linear response over 40–280 μM, with a sensitivity of 0.019639 μA μM^{-1} , an LOD of 75.72 μM, and an LOQ of 252.41 μM. The sensor showed good anti-interference performance against common matrix species and acceptable stability, repeatability, and reproducibility. Application in spiked milk samples produced recoveries of 95.6–97.5%, supporting the preliminary practical applicability of the SnO_2-PANI/MCPE platform for SDZINE detection.

1. Introduction

Recent advances in materials chemistry have accelerated the design of functional materials for use in therapeutics, diagnostics, electronics, catalysis, and energy storage [1–3]. Among these, metal oxide nanomaterials have attracted sustained interest because of their high surface area, intrinsic catalytic activity, and favourable electron-transport characteristics, which can be leveraged in biosensing and pollutant monitoring platforms [4–7].

Metal oxide systems such as Fe_3O_4, Fe_2O_3, SnO_2, ZnO, TiO_2, and Cu_2O are widely explored in sensor design due to their thermal and chemical stability, comparatively low toxicity, and ability to promote interfacial electron transfer [8–10]. These features translate into broad utility in electrochemical devices and sensors, where accessible active sites and improved catalytic efficiency are required for measurable signal amplification [11–19].

In the present work, SnO_2 was selected over other commonly used oxides such as ZnO, CuO, and TiO_2 because of its favourable combination of semiconducting behaviour, catalytic activity, chemical stability, relative affordability, and environmental compatibility. SnO_2 is an n-type semiconductor with a wide band gap (~3.6 eV at room temperature) [20,21]and exhibits multiple valence states and oxygen vacancies that promote redox activity. Consequently, SnO_2-based nanostructures have been employed in electrochemical energy [22] and sensing applications [23–28], with the additional advantages of relative affordability and environmental compatibility [29].

Combining SnO_2-based interfaces with conductive polymers (CPs) such as polyaniline (PANI), polypyrrole (PPy), and poly(3,4-ethylenedioxythiophene) (PEDOT), is a popular method for further improving conductivity [30] and providing electroactive or adsorptive sites via straightforward synthesis routes [31–33]. PANI is attractive because it exhibits multiple oxidation states, with the emeraldine salt form being the most electroactive and conductive [34]. These characteristics have supported PANI's widespread use in sensing, corrosion protection, and electrocatalytic systems [35]. SnO_2–PANI nanocomposites synergistically combine the conductivity of PANI with the

* Corresponding author.
E-mail addresses: chem.swastika@bldeacet.ac.in, drswastika@yahoo.com (S. N. Das).

https://doi.org/10.1016/j.nxmate.2026.102399
Received 1 March 2026; Received in revised form 19 May 2026; Accepted 29 May 2026

catalytic activity of SnO_2, resulting in improved sensing capability [36]. Interfacial coupling between semiconductor oxides and conductive polymers can promote charge transport across the composite in terms of favourable band alignment and junction formation [37,38], influencing structural and electrochemical characteristics relevant to sensing [39–42]. Although SnO_2–PANI nanocomposite systems have been explored for sensing gases and small molecules, including ethanol, ammonia, and ethephon [43–45] their application in pharmaceutical sensing, particularly for antibiotics such as SDZINE remains largely unexplored. The present study addresses this gap by developing a SnO_2–PANI/MCPE platform for SDZINE detection and evaluates its applicability in spiked milk samples. A summarised overview of the key research gaps in existing SDZINE detection approaches and how the present work addresses them is provided in supplementary Table ST2. To bridge the gap and from a functional materials perspective, the present work demonstrates how a semiconductor metal oxide, SnO_2 and a conducting polymer, PANI, can be integrated to generate a practical electrochemical interface. In this hybrid system, SnO_2 contributes catalytic surface activity, oxygen-vacancy-assisted redox behaviour, and nanoscale active sites, while PANI improves conductivity, charge mobility, and analyte–surface interaction. Thus, the SnO_2–PANI/MCPE platform supports the broader development of next-generation, low--cost, and application-oriented functional materials for electrochemical sensing.

Due to its broad-spectrum antibacterial action and low cost, SDZINE, a synthetic antibiotic of the sulfonamide class, is frequently employed in both human and veterinary medicine [46]. Structurally (Fig. 1), it contains a pyrimidine ring linked to a 4-aminobenzenesulfonamido group, and it has been used in a range of bacterial and parasitic infections [47–49]. However, residual SDZINE in animal-derived foods like milk and meat, raises safety concerns, including hypersensitivity reactions and other adverse effects associated with unnecessary exposure [50,51]. Accordingly, regulatory frameworks impose limits on sulfonamide residues in foods of animal origin. The European Union has established a combined maximum residue limit for sulfonamides that is commonly expressed at 100 ng/g (equivalent to 100 μg/kg) in relevant animal-derived products [52], and some standards specify stringent limits for SDZINE in milk [53,54]. Environmental monitoring has also reported SDZINE contamination in aquatic systems, underscoring the need for sensitive and reliable detection strategies for both food-safety and environmental surveillance [55,56].

Several analytical techniques have been developed for SDZINE detection, including UV-Visible spectrophotometry [57], chromatographic approaches [58], capillary electrophoresis [59], and tandem mass spectrometry [60]. Although these conventional techniques offer high sensitivity and specificity, their routine use is limited by the need for expensive instrumentation, skilled personnel, laborious sample preparation, and relatively time-consuming analytical procedures [61–63]. In this context, electrochemical sensing has emerged as a promising alternative for antibiotic residue monitoring because it offers simplicity, portability, rapid analysis, low cost, and high sensitivity,

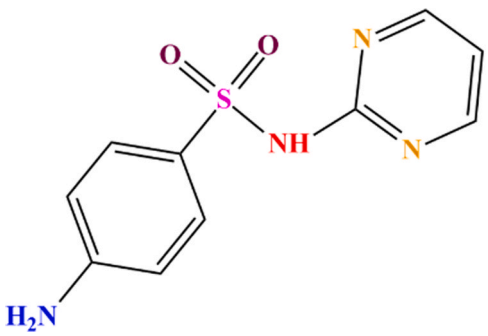

Fig. 1. Structure of SDZINE.

making it attractive for real-time monitoring of pharmaceutical residues in food and biological matrices [64]. In addition, nanocomposite-modified electrodes can improve sensing performance by enhancing electron transfer, increasing active surface area, and strengthening analyte–electrode interactions [65]. Although multiple electrochemical sensors for SDZINE have been reported using chemically modified carbon electrodes [66], many reported electrochemical SDZINE sensors rely on relatively complex modifier systems, molecular imprinting, or advanced nanostructures, which may limit ease of fabrication and routine use. Therefore, a simpler and more cost-effective electrode architecture that maintains acceptable sensitivity, selectivity, and real-sample applicability is still required. In this regard, SnO_2–PANI nanocomposites are attractive as well as underexplored sensing material on a carbon based electrode system. To the best of our knowledge, the use of a SnO_2–PANI/MCPE platform for drug detection has not yet been systematically explored. The novelty of the present work lies not in claiming the lowest reported detection limit but in demonstrating a simple, low-cost, SnO_2–PANI nanocomposite-based carbon paste electrode that combines an improved electrocatalytic response, good selectivity, and practical applicability for SDZINE detection in a milk matrix.

2. Materials and methods

2.1. Apparatus

The morphological and elemental characteristics of the synthesised nanomaterials were investigated using scanning electron microscopy (SEM) coupled with energy-dispersive X-ray spectroscopy (EDX) on a JEOL JSM-IT500LA instrument at the Sophisticated Analytical Instrument Facility (SAIF), Karnatak University, Dharwad, India. To examine the crystallographic structure, phase purity, and lattice parameters of the materials, powder X-ray diffraction (XRD) was performed using a Rigaku SmartLab SE diffractometer with Cu Kβ1D radiation.

A CHI 619E electrochemical workstation with a standard three-electrode setup was used to perform electrochemical experiments. The SnO_2-PANI/MCPE served as the working electrode in this configuration, while a platinum wire served as the counter electrode and a saturated calomel electrode (SCE) as the reference electrode. All measurements were performed in a typical laboratory setting at room temperature. The pH of the solutions used in the electrochemical analysis was determined using a calibrated digital pH meter (Elico LI120).

2.2. Chemicals

All chemicals employed in this investigation were of analytical grade and did not require any additional purification. Sigma-Aldrich was the source of SDZINE. Himedia provided stannous chloride dihydrate ($SnCl_2{\cdot}2H_2O$), sodium hydroxide (NaOH), aniline hydrochloride ($C_6H_5NH_2{\cdot}HCl$), ammonium peroxydisulfate $(NH_4)_2S_2O_8$, monosodium dihydrogen phosphate (NaH_2PO_4), and disodium hydrogen phosphate (Na_2HPO_4). All analyses were conducted in 0.2 M PBS (pH 7.4). For consistency and to remove interfering ions, double-distilled water was used in all the experiments and solution formulations.

2.3. Synthesis of nanoparticles

The traditional co-precipitation process was followed to synthesize the SnO_2 nanoparticles. First, a transparent precursor solution was prepared by mixing 2.256 g of $SnCl_2.2H_2O$ with 500 mL of distilled water. Separately, 0.4 g of NaOH was dissolved in 500 mL of distilled water. A magnetic stirrer was used to continuously stir the $SnCl_2$ solution as it was transferred to a 1 L beaker and combined with 100 mL of ethanol. Subsequently, NaOH solution was gradually added to the $SnCl_2$ solution until the pH of the mixture approached 8, facilitating the formation of a white precipitate [67]. The resulting suspension was allowed

to stand undisturbed overnight to ensure complete precipitation of the particles. The following day, the supernatant was carefully decanted, and the precipitate was washed thrice with distilled water to remove residual ions. After cleaning, the precipitate was filtered on Whatman filter paper, then transferred to a crucible and calcined at 250 °C for 2–3 h. For subsequent characterisation and electrode fabrication, the finished product was collected the following day and stored.

Polyaniline (PANI) was synthesised via the oxidative polymerisation of $C_6H_5NH_2{\cdot}HCl$ using $(NH_4)_2S_2O_8$ as the oxidising agent. In this process, 2.59 g of $C_6H_5NH_2{\cdot}HCl$ was mixed with 50 mL of distilled water to prepare a 0.2 M solution. Simultaneously, 5.71 g of $(NH_4)_2S_2O_8$ was dissolved in 50 mL of distilled water to obtain a 0.25 M solution. Both solutions were equilibrated at room temperature for one hour. After this period, the two solutions were mixed in a clean beaker, stirred briefly to initiate the polymerisation reaction, and left undisturbed overnight. By the next day, a green precipitate, indicative of emeraldine salt formation, had settled. To remove unreacted monomers and oligomers, the precipitate was filtered, washed with 0.2 M HCl, and then with acetone. To create the final powder, the purified PANI was first allowed to dry in open air and then oven-dried at 60°C. This powder was then kept for use in electrode modification.

2.4. Fabrication of the electrodes

The BCPE was prepared from a paste of fine graphite powder and silicone oil in a weight ratio of 70:30 using a mortar and pestle [68,69]. The paste was then pressed into the hollow cavity of a Teflon tube, and a copper wire was inserted to ensure electrical contact with the electrode. The electrode surface was polished with glossy paper before use. To fabricate the modified electrode, equal amounts (0.001 g each) of the synthesised SnO_2 and PANI nanoparticles were dispersed in 1 mL of double-distilled water. A consistent dispersion was achieved by ultrasonication of the resultant suspension for 30–45 min. After combining equal volumes of each dispersion, they were further sonicated to guarantee homogeneity; thus, the SnO_2–PANI nanocomposite suspension was prepared. Subsequently, 10, 20, and 30 μL of the SnO_2–PANI nanocomposite suspension were drop-casted on the surface of the BCPE and dried under ambient conditions. Electrochemical analysis by cyclic voltammetry showed that 20 μL of the modifier yielded an optimal current response. At this volume, the nanocomposite formed a uniform thin film that enhanced electron transfer without hindering surface conductivity.

2.5. Preparation of a real sample

To evaluate the practical applicability of the fabricated SnO_2-PANI/MCPE, a real sample analysis was performed using raw domestic milk. A 100 mL volumetric flask was filled with 10 mL of unprocessed milk and diluted to the appropriate volume with double-distilled water. The mixture was then sonicated for 5–10 min to ensure homogeneity and to break down any aggregated proteins or particulates that might interfere with the electrochemical analysis. Following sonication, appropriate aliquots were drawn from the stock solution and further diluted with 0.2 M PBS at pH 7.4 to prepare the working solutions. These diluted samples were transferred to an electrochemical cell for analysis using CV and DPV. To confirm the recovery and performance of the sensor in a real matrix, spiking experiments were performed by adding known concentrations of SDZINE to the milk sample, and the recovery percentages were calculated.

3. Results and discussions

3.1. Characterization of SnO_2 nanoparticles by SEM-EDX analysis

The surface morphologies of the synthesised SnO_2 nanoparticles and SnO_2-PANI nanocomposite were examined using scanning electron microscopy (SEM). The SEM image of the SnO_2 nanoparticles at X2000 magnification reveals a granular surface structure with a relatively uniform particle distribution (Fig. 2A). The particles appeared quasi-spherical and loosely agglomerated, which is typical of nanomaterials synthesised via co-precipitation methods. The morphology suggests a high surface area, which is beneficial for electrochemical sensing applications because of the enhanced active surface interaction.

The SEM image of the SnO_2-PANI nanocomposite at X2000 magnification, as shown in Fig. 2B, reveals the presence of agglomerates of spherical SnO_2 nanoparticles on the surface of the PANI particles. This suggests that the composite is extremely microporous, with an enhanced liquid–solid interfacial area that provides additional sites for ion insertion and extraction, resulting in an elevated heterogeneous reaction rate.

Energy-dispersive X-ray spectroscopy (EDX) analysis was performed to confirm the elemental composition of the nanomaterial. The EDX spectrum shown in Fig. 3A clearly indicates that the sample contains tin (Sn) and oxygen (O) as the dominant elements, confirming the formation of SnO_2 nanoparticles. The quantitative EDX data revealed that tin (Sn) accounted for 58.41 wt% and 76.31 at%, and oxygen (O) accounted for 37.56 wt% and 15.99 at%. These values are in good agreement with the stoichiometry of SnO_2, thereby validating the successful synthesis of the desired SnO_2 nanoparticles without significant impurities [70].

The EDX spectrum shown in Fig. 3B indicates that the sample contains carbon, oxygen, tin, and chlorine as the dominant elements, confirming the formation of the SnO_2-PANI nanocomposite. The quantitative EDX data reveal that carbon (C) accounts for 63.27 wt% and 78.84 at%, oxygen (O) accounts for 17.03 wt% and 15.93 at%, tin (Sn) accounts for 10.79 wt% and 1.36 at%, and chlorine (Cl) accounts for 6.57 wt% and 2.78 at%.

3.2. Powder X-Ray diffractometer analysis

X-ray diffraction (XRD) was used to examine the crystal structure and phase purity of the synthesised SnO_2 nanoparticles. As shown in Fig. 4A, prominent peaks at 2θ values of approximately 26.7°, 33.8°, 51.8°, 54.6°, 58.2°, 61.7°, 65.1°, and 78.8° were observed, which can be indexed to the (110), (101), (211), (220), (002), (310), (301), and (321) crystallographic planes, respectively. These reflections are in good agreement with the tetragonal rutile phase of SnO_2 (JCPDS card No. 41–1445), confirming the successful formation of crystalline SnO_2 without any detectable secondary impurity phases [71].

Similarly, the XRD pattern of PANI (Fig. 4B) showed broad peaks at 2θ values of 8.5° and 25.36°, corresponding to the (001) and (200) planes, respectively. The crystallite size was found to range from approximately 2.0–4.6 nm (Table 1) [72].

The typical XRD characteristic peaks of the SnO_2–PANI nanocomposite (Fig. 4C) were observed at 2θ values of 26.5°, 33.7°, 37.9°, 51.7°, 54.6°, 57.8°, 61.8°, 65.2°, 71.6°, 78.4°, and 83.7°. These peaks correspond to the (110), (101), (200), (211), (220), (002), (310), (112), (202), (321), and (222) planes, respectively, and are consistent with the characteristic diffraction pattern of SnO_2 [73]. No additional impurity phases were observed. The slight deviation of peak positions from the standard SnO_2 values may be attributed to the incorporation of SnO_2 within the PANI matrix and possible interfacial interaction between the two components (Table 1). This suggests that the presence of PANI may influence the preferred orientation and crystalline environment of SnO_2 in the nanocomposite. No distinct PANI-related diffraction peaks were observed in the SnO_2–PANI nanocomposite, which may be due to the relatively low amount and low crystallinity of PANI in the composite.

The crystallite sizes at different 2θ values were obtained from the profile-fitting analysis of the XRD data and are presented in Table 1. The estimated crystallite sizes ranged from approximately 1.9–9.3 nm, with an average value of approximately 5.5 nm. These values represent XRD-derived crystalline domain sizes and should not be interpreted as direct particle-size measurements. The variation in crystallite size across

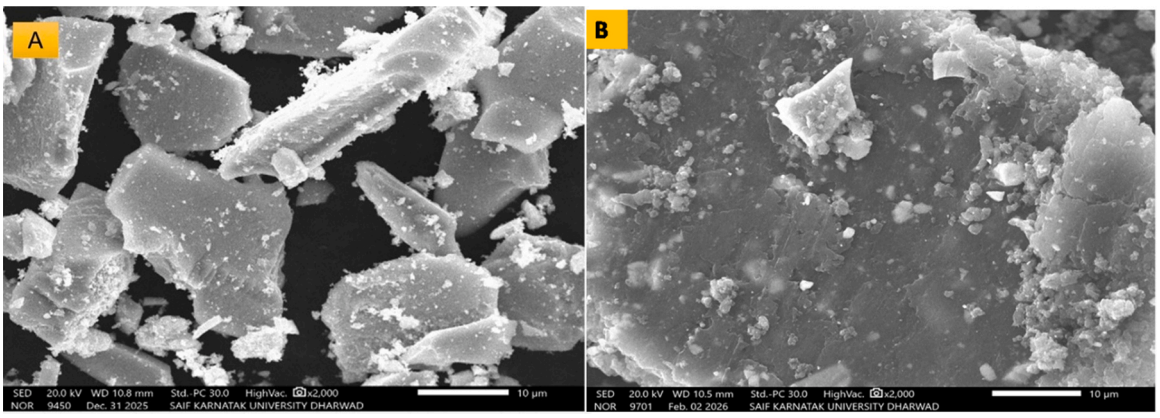

Fig. 2. The SEM images with different magnification **A)** SnO_2 nanoparticles at X2000 **B)** SnO_2–PANI nanoparticles at X2000 at landing Voltage 20.0 kV.

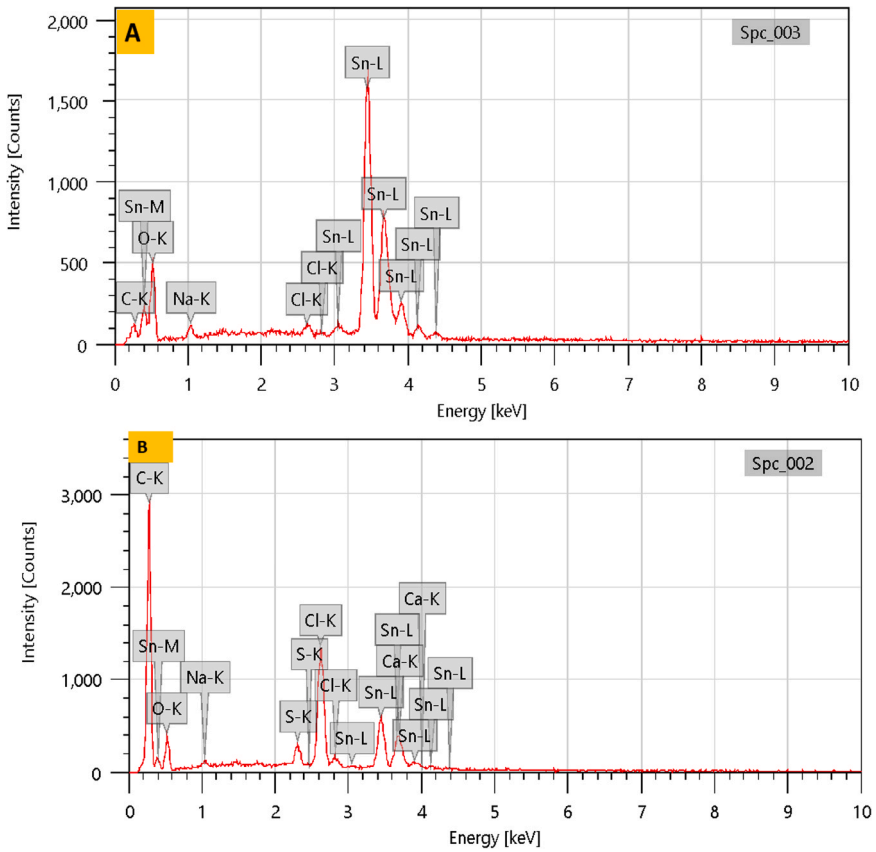

Fig. 3. EDX spectra of **A)** SnO_2 and **B)** SnO_2 – PANI nanocomposite.

different diffraction planes may be related to differences in crystalline domain orientation and peak-broadening behaviour. The absence of additional diffraction peaks suggests good phase purity of SnO_2 within the detection limit of XRD. Overall, the XRD findings support the formation of nanocrystalline SnO_2 with a rutile tetragonal structure, while SEM-EDX provides complementary evidence regarding surface morphology and elemental composition. The nanocrystalline nature of SnO_2 may provide accessible active sites and support charge transfer, making it suitable for integration into the SnO_2–PANI composite sensor platform.

3.3. FTIR characterisation of SnO_2-PANI/MCPE

The FTIR spectrum of the SnO_2–PANI/MCPE (Fig.S1) shows characteristic absorption bands corresponding to SnO_2, PANI, and the carbon paste matrix. Detailed FTIR peak assignments are provided in Supplementary Table ST1. The absorption band around 561.29 cm^{-1}, along with bands at 709.80, 678.94, and 653.87 cm^{-1}, may be assigned to Sn–O and Sn–O–Sn vibrations, supporting the presence of SnO_2 in the composite. The bands observed at 817.82, 848.68, and 906.54 cm^{-1} correspond to aromatic C–H bending vibrations of PANI. The bands at 1234.44 and 1255.66 cm^{-1} are attributed to C–N stretching vibrations, while the bands at 1508.33 cm^{-1} and 1541.12–1560.41 cm^{-1} correspond to benzenoid and quinoid ring stretching vibrations of PANI, respectively. These PANI-related bands support the retention of the emeraldine-type conducting polymer backbone in the composite. The band near 1047.35 cm^{-1} may be associated with Si–O–Si stretching from silicone oil used as the binder in the

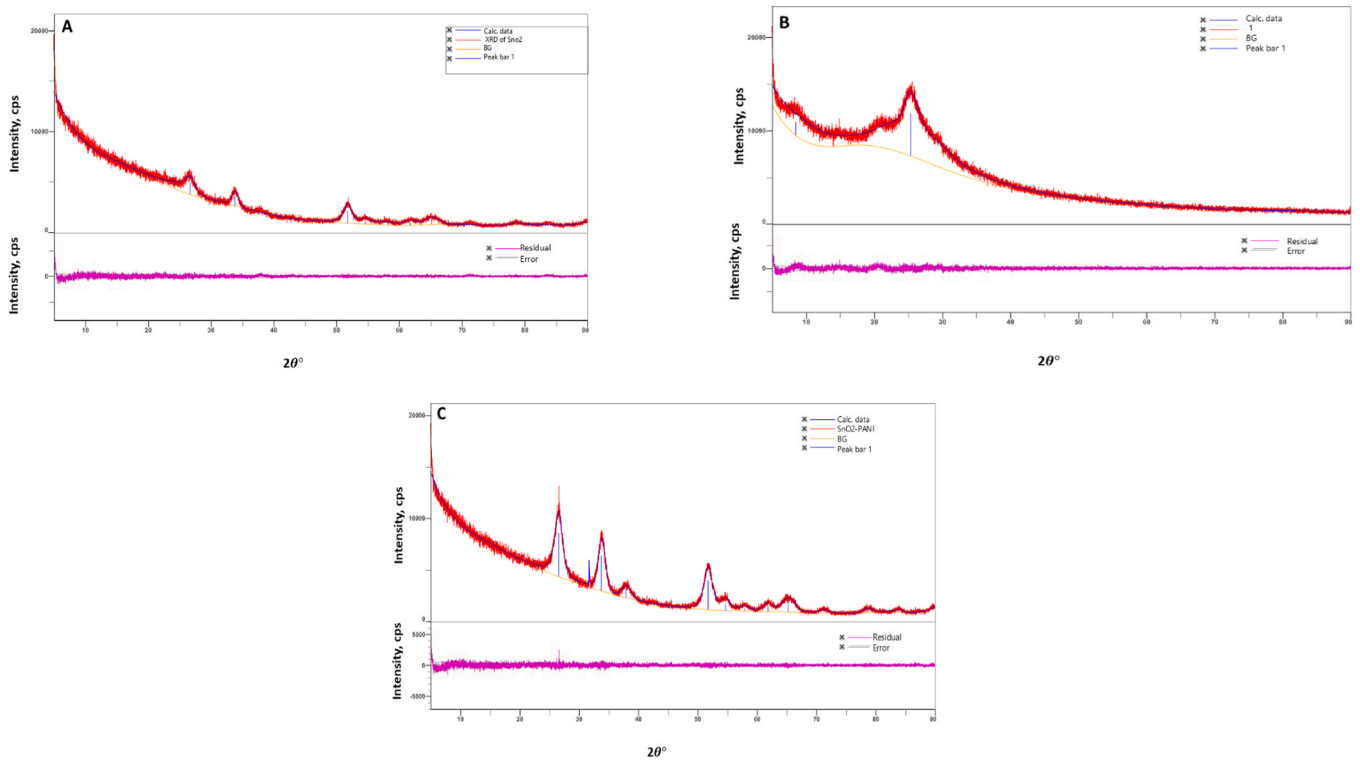

Fig. 4. XRD spectra of **A)** SnO_2 **B)** PANI **C)** SnO_2-PANI.

Table1
XRD data of SnO_2, PANI and SnO_2-PANI.

	SnO_2 nanoparticles	**PANI**		**SnO_2 – PANI nanocomposite**	
2θ (°)	**Crystallite size (nm)**	**2θ (°)**	**Crystallite size (nm)**	**2θ (°)**	**Crystallite size (nm)**
26.7	3.6	8.5	4.6	26.5	5.4
33.8	7.2	25.3	2.0	33.7	6.2
51.7	5.8			37.9	5.0
54.6	9.3			51.7	5.5
58.2	1.8			54.6	6.2
61.7	5.1			57.8	5.9
65.1	3.6			61.8	5.6
78.8	7.0			65.2	3.9
				71.6	7.1
				78.4	6.1
				83.7	8.8

carbon paste electrode. The broad bands around 3649.32 and 3738.05 cm^{-1} are attributed to O–H stretching from surface hydroxyl groups or adsorbed moisture, while the band at 2358.94 cm^{-1} may arise from atmospheric CO_2. Overall, the FTIR spectrum supports the coexistence of SnO_2 and PANI components in the modified carbon paste electrode and provides additional evidence for successful composite formation. This is relevant for SDZINE sensing because SnO_2 can contribute surface-active catalytic sites for electro-oxidation, whereas PANI provides conductive pathways that facilitate interfacial charge transfer.

3.4. Electrochemical behaviour of SDZINE at the various modified electrodes

The electrochemical behaviour of SDZINE at different electrode surfaces was evaluated using cyclic voltammetry in 0.2 M PBS at pH 7.4. Comparative studies were performed using BCPE, SnO_2-MCPE, PANI-MCPE, and SnO_2–PANI/MCPE in the presence of 0.1 mM SDZINE, and the corresponding anodic peak potentials (E_{pa}) and anodic peak currents (I_{pa}) are presented in Table 2. The SnO_2–PANI/MCPE exhibited the maximum anodic peak current (-2.811×10^{-6} A), compared to BCPE (-2.643×10^{-7}), corresponding to an approximately 10.6 fold increase in current response, while SnO_2-MCPE and PANI-MCPE individually produced a moderate enhancement in the SDZINE oxidation response. The anodic peak potential also shifted slightly from 0.8776 V at BCPE to 0.8696 V at SnO_2–PANI/MCPE. This slight negative shift in E_{pa}, together with the marked current enhancement, indicates improved electrocatalytic oxidation of SDZINE at the nanocomposite-modified electrode surface. The improved response of the SnO_2–PANI/MCPE may be attributed to the synergistic contribution of the SnO_2 surface-active catalytic sites and PANI conductive pathways, which together facilitate interfacial charge transfer during SDZINE oxidation. Fig. 5A shows the oxidation voltammograms of SDZINE at the BCPE and SnO_2–PANI/MCPE.

No well-defined cathodic peak corresponding to SDZINE reduction was observed in the reverse scan under the present experimental conditions, suggesting that SDZINE oxidation at the electrode surface is electrochemically irreversible or is followed by a rapid chemical transformation of the oxidised product. Therefore, peak separation (ΔE_p), which is usually used for reversible redox couples, was not calculated for SDZINE oxidation. Instead, the mechanistic interpretation was based on the anodic peak potential shift, current enhancement, scan rate dependence, and pH-dependent behaviour.

Table 2
Comparison of responses of different modifiers.

Modifiers	**E_{pa} (V)**	**I_{pa} (A)**
BCPE	0.8776	-2.643×10^{-7}
BCPE + SnO_2	0.8660	-2.029×10^{-6}
BCPE + PANI	0.8585	-1.162×10^{-6}
BCPE + SnO_2 + PANI	0.8696	-2.811×10^{-6}

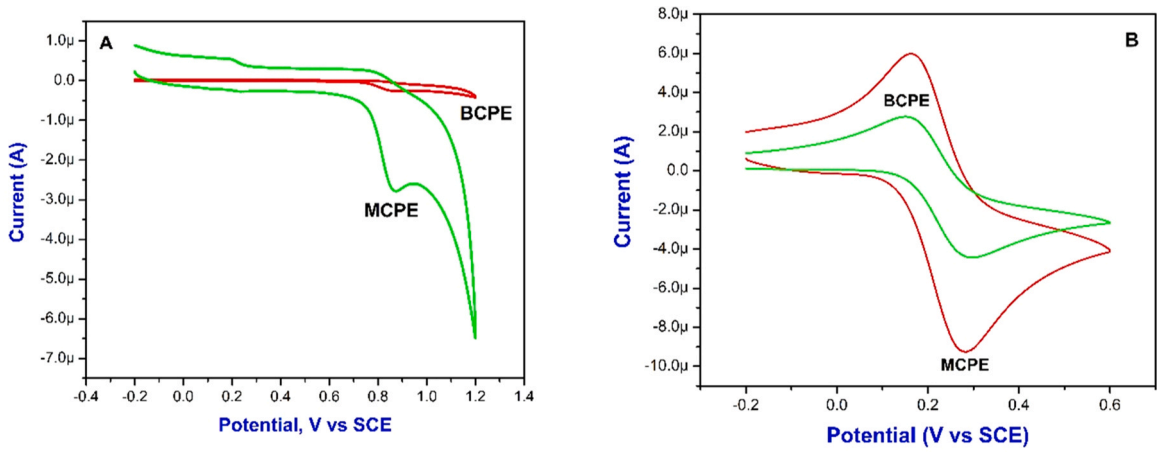

Fig. 5. (A) Electro oxidative behaviour of 0.1 mM SDZINE at the BCPE and at SnO_2-PANI/MCPE in 0.2 M PBS (pH 7.4) at a scan rate of 0.05 V/s. **(B)** Electro oxidative behaviour of 1.0 mM potassium ferrocyanide at the BCPE and SnO_2-PANI /MCPE in 0.1MKCl recorded at a scan rate of 0.05 V/s.

3.5. Electrochemical oxidation of the standard potassium ferrocyanide system on SnO_2-PANI/MCPE

To investigate the electrochemical characteristics of the SnO_2–PANI/MCPE, we employed a freshly prepared probe solution of 1.0 mM potassium ferrocyanide in 0.1 M KCl in an electrochemical cell. The cyclic voltammograms acquired at the BCPE and SnO_2-PANI/MCPE during the oxidation of 1.0 mM potassium ferrocyanide at a scan rate of 0.05 V/s are shown in Fig. 5B. The resulting voltammograms showed a significant enhancement in the current response at the SnO_2-PANI/MCPE surface. The peak-to-peak separation $(\Delta E_p)$and peak current ratio (I_{pa}/I_{pc}) of the ferrocyanide redox probe were also evaluated to understand the interfacial electron-transfer behaviour of the electrode. At the BCPE, $E_{pa}$and E_{pc}were observed at 0.2959 V and 0.1544 V, respectively, giving a $\Delta E_p$of 141.5 mV and an I_{pa}/I_{pc}ratio of 1.611. In contrast, the SnO_2-PANI/MCPE showed $E_{pa}$and E_{pc}values of 0.2826 V and 0.1618 V, respectively, with a reduced ΔE_p of 120.8 mV and an I_{pa}/I_{pc}ratio of 1.560. The reduction in ΔE_p, together with the enhanced peak current response and higher electroactive surface area reported for SnO_2-PANI/MCPE, indicates improved charge-transfer kinetics at the modified electrode surface. However, since the ΔE_pvalues remain higher than the theoretical value expected for a fully reversible one-electron redox process, the ferrocyanide response may be described as quasi-reversible rather than fully reversible.

The total active surface area was calculated using the Randles-Sevcik Eq. (1)

$$Ip = (2.69\times10^5)\, n^{3/2} A\, D^{1/2}\, C_0 \nu^{1/2} \quad (1)$$

In the above equation, Ip, C_0, n, D,ν, A are the peak current, concentration of the electroactive species (mol cm^{-3}), number of electrons exchanged, diffusion coefficient ($cm^2 s^{-1}$), scan rate (V/s) and electroactive surface area (cm^2), respectively. The electroactive surface area of SnO_2-PANI/MCPE was found to be at its maximum at 0.01514 cm^2, surpassing that of BCPE (0.0097 cm^2). This result confirms that nanocomposite modification enhances the electrochemical surface area and charge-transfer capability of the electrode [74]. The proposed electro-oxidation mechanism of SDZINE is shown in Scheme 1.

Since intermediate species were not experimentally identified by LC-MS, GC-MS, controlled-potential electrolysis, or in situ spectroelectrochemistry, the proposed pathway should be considered tentative and based only on the observed electrochemical behaviour.

3.6. The effect of scan rate variation on electro-oxidation of SDZINE

The CV technique was used to investigate the impact of the scan rate on the electrochemical oxidation of SDZINE at the SnO_2-PANI/MCPE over a range of scan rates from 0.04 to 0.52 V/s. The anodic peak current (I_{pa}) increased with increasing scan rate from 0.04 to 0.52 V/s, as shown in Fig. 6 A, confirming the scan rate-dependent oxidation of SDZINE. Fig. 6B illustrates the linear correlation between I_{pa} and the scan rate (ν) with the following regression Eq. (2):

$$I_{pa\,SDZINE} = 1.56304\nu - 1.6304 \qquad (R^2 = 0.9995) \quad (2)$$

Similarly, a plot of I_{pa} versus $\nu^{1/2}$ also demonstrated a straight-line

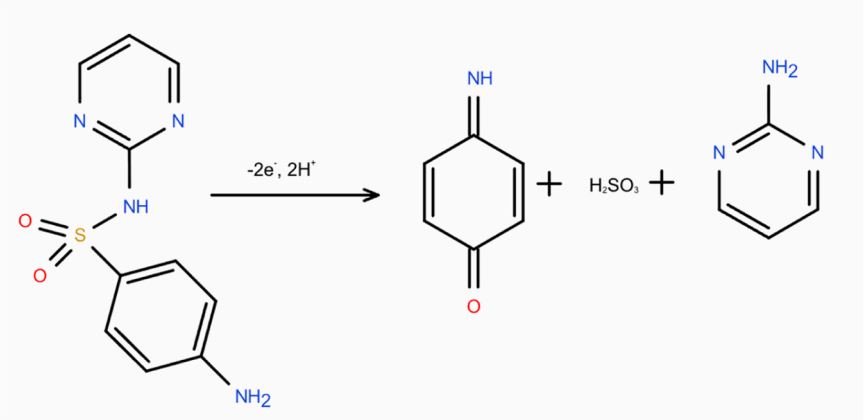

Scheme 1. Proposed electro oxidation pathway of SDZINE at SnO_2-PANI/MCPE electrode surface.

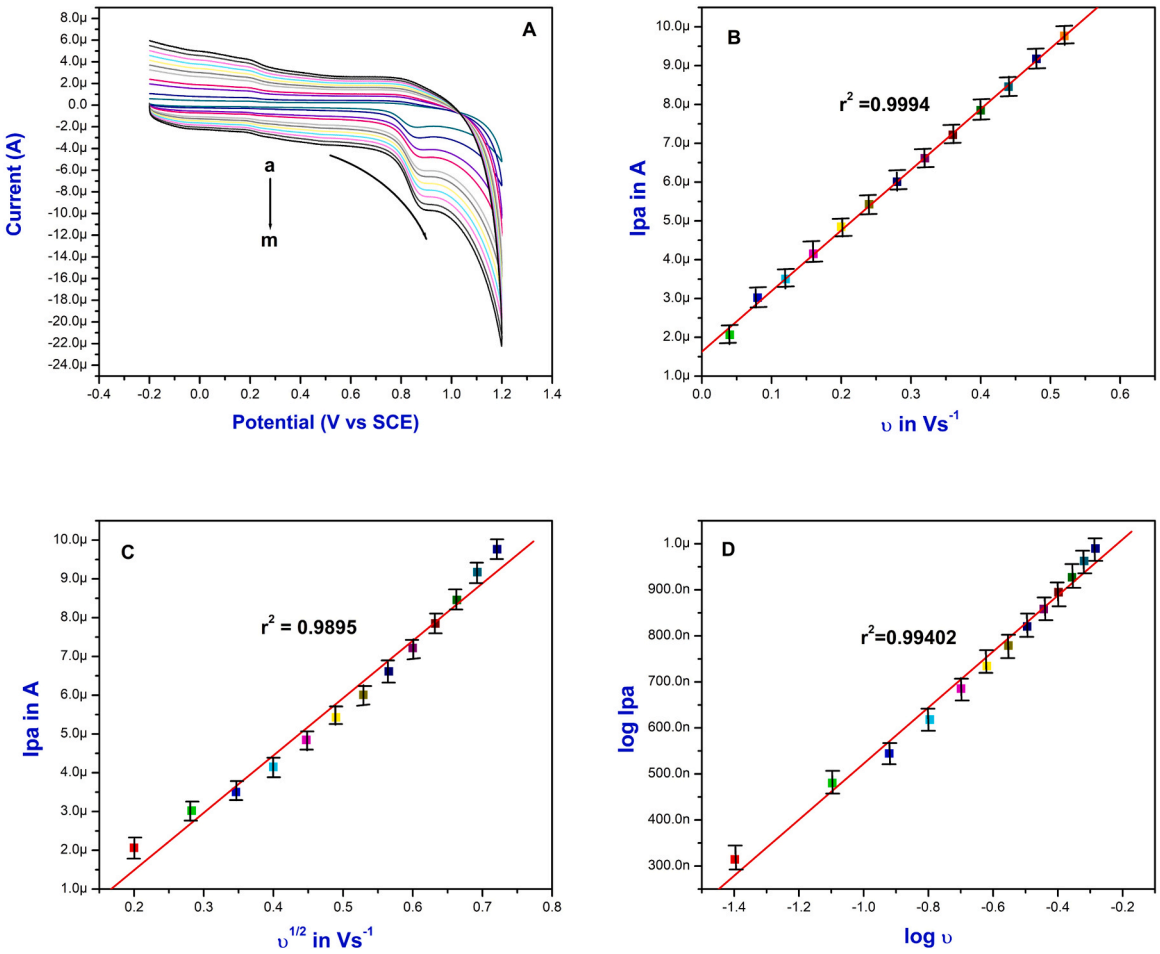

Fig. 6. **(A)** Cyclic voltammogram of 0.1 mM SDZINE at the MCPE at different scan rates (a−0.04 V/s to m−0.52 V/s). **(B)** Plot of I_{pa} versus ν for SDZINE. **(C)** Plot of I_{pa} versus $\nu^{1/2}$ for SDZINE. **(D)** Plot of log I_{pa} versus logν for SDZINE.

trend shown in Fig. 6C and described by the Eq. (3)

$$I_{pa_{SDZINE}} = 1.4793\nu^{1/2} + 1.47003 \qquad (R^2 = 0.9896) \qquad (3)$$

However, to further elucidate the dominant control mechanism, a plot of the logI_{pa} versus logν was plotted (Fig. 6D), and the linear Eq. (4) was obtained.

$$\log\ (I_{pa}/\mu A) = 0.608\ (\log V/s) + 1.13 \qquad (R^2 = 0.994) \qquad (4)$$

A slope close to 0.5 generally indicates diffusion-controlled behaviour, whereas a slope close to 1.0 indicates adsorption-controlled behaviour [75]. The obtained value suggests a mixed diffusion–adsorption-controlled process with a significant adsorption contribution.

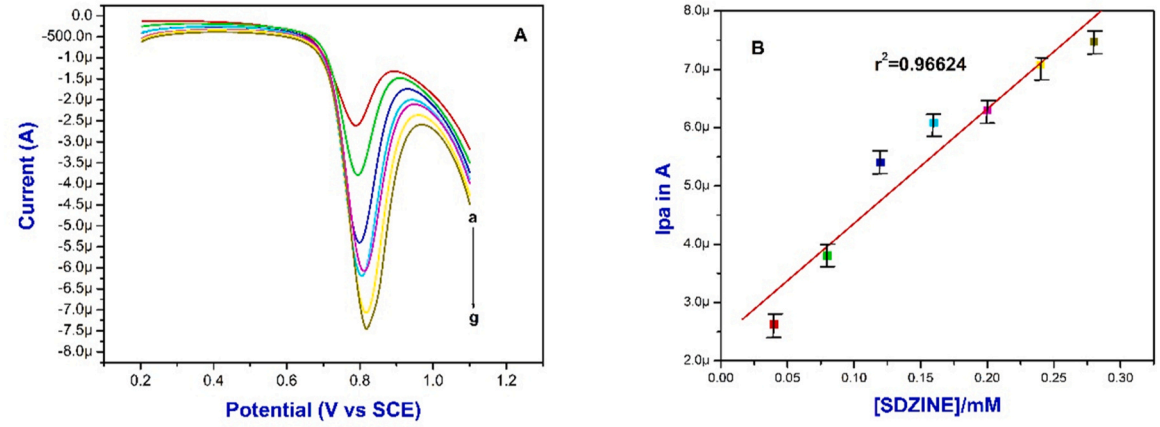

Fig. 7. **(A)** Differential pulse voltammograms for increase in concentration of Sulphadiazine (a- 0.04 mM to g −0.28 mM). **(B)** Calibration plot of Ipa versus concentration of Sulphadiazine.

3.7. Effect of concentration of SDZINE at SnO_2 -PANI/MCPE

To evaluate the electrocatalytic performance of the SnO_2-PANI/MCPE for SDZINE detection, differential pulse voltammetry (DPV) was performed at varying analyte concentrations. Fig. 7A illustrates the DPV responses obtained as the SDZINE concentration was incrementally increased from 0.04 to 0.28 mM (40 μM to 280 μM). A steady increase in the anodic peak current (I_{pa}) confirmed a good electrochemical contact between the analyte and the modified electrode surface with increasing SDZINE concentration. Over the measured range, the accompanying calibration curve (Fig. 7B) shows a linear connection between I_{pa} and SDZINE concentration described by the regression Eq. (5):

$$I_{pa}(\mu A) = 0.019639 \quad C_{SDZINE}(\mu M) + 2.3942 \left(R^2 = 0.9662\right) \tag{5}$$

The performance of the SnO_2-PANI/MCPE sensor was further evaluated by calculating the limit of detection (LOD), limit of quantification (LOQ) and sensitivity were calculated as follows:

$$LOD = \frac{3\sigma}{S} = \frac{3 \times 0.49571}{0.019639}$$

$$LOD = 75.72\ \mu M$$

$$LOQ = \frac{10\sigma}{S} = \frac{10 \times 0.49571}{0.019639}$$

$$LOQ = 252.41\ \mu M$$

The LOD and LOQ were found to be 75.72 μM and 252.41 μM, respectively.

The sensitivity was found to be 0.019639 μA μM^{-1} and the area-normalised sensitivity was found to be 1.29 μA $\mu M^{-1} cm^{-2}$ indicating the sensor's acceptable sensitivity and the ability to detect SDZINE at trace levels. The newly developed SnO_2-PANI/MCPE sensor's ability was also compared with other previously reported electrochemical sensors for SDZINE detection (Table 3). The LOD obtained in the present work is not the lowest among all reported electrochemical SDZINE sensors, as some advanced nanostructured and molecularly imprinted systems have achieved lower detection limits. However, the SnO_2–PANI/MCPE provides a favourable balance between analytical performance and practical usability. The electrode is simple to fabricate, uses inexpensive and relatively environmentally benign materials, exhibits enhanced current response compared with BCPE. These attributes suggest that the SnO_2-PANI/MCPE is an attractive platform for the accurate and efficient electrochemical determination of SDZINE in pharmaceutical and food samples. Recent reports on SDZINE electrochemical sensing [66,76–80] show a clear trend toward highly engineered recognition and signal-amplification platforms, including molecularly imprinted polymers, metal/metal-oxide nanocomposites, MXene/silver nanowire systems, and carbon-supported hybrid nanostructures. Some of these recent sensors have achieved lower detection limits than the present SnO_2-PANI/MCPE, such as CuNPs/MIP, $MnCo_2O_4$/P-doped g-C_3N_4/GCE, Nb_2CTx/AgNWs-MIP/GCE, SDZ-MIP/APTES-ITO, differential ratiometric MIP sensors, and CNFs@Sb_2O_3/GCE-based systems. However, these platforms often involve more complex modifier synthesis, molecular imprinting, ratiometric design, or advanced electrode substrates. In contrast, the present SnO_2-PANI/MCPE offers a simpler carbon paste electrode architecture with low-cost materials, easy fabrication, improved anodic response compared with the bare and individually modified electrodes, acceptable analytical sensitivity, good selectivity, and successful recovery in spiked milk samples. Therefore, the contribution of the present work lies not in achieving the lowest reported LOD, but in providing a practical balance between sensitivity, fabrication simplicity, cost-effectiveness, and real-sample applicability. Also, we would like to add that the present sensor showed a linear response from 0.04 to 0.28 mM (40–280 μM), this range is higher than typical regulatory residue limits for sulfonamides in food matrices. Therefore, the present study should be considered a proof-of-concept electrochemical sensing platform, and further optimisation including lower calibration ranges, sample preconcentration, and matrix-specific validation will be required for residue-level food-safety monitoring.

3.8. The effect of pH on SDZINE detection

The pH of the supporting electrolyte is a critical parameter that can significantly influence the electrochemical behaviour of analytes [87]. To investigate its effect on the electro-oxidation of SDZINE, cyclic voltammetry was performed over a pH range of 5.5–8.0. The measurements were carried out at a scan rate of 0.05 V/s using the SnO_2-PANI/MCPE (Fig. 8A).

The pH-dependent study supports the mechanistic interpretation of SDZINE oxidation. With increasing pH, the anodic peak potential shifted toward less positive values, indicating proton involvement in the oxidation process. The slope of the E_{pa}versus pH plot (Fig. 8B) was

Table 3
Comparison of the detection limit for SDZINE with different modifiers and techniques.

Modified Electrode	Technique	Linear Range (μM)	Limit of Detection (LOD in μM)	References
Molecular imprinted polymer – CPE	DPV	0.2 −100 μM	0.14	[52]
GCE	SWV	62.7–340 μM	10.9	[64]
MWCNT– GCE	CV	10–2000 μM	7.13	[81]
MIP/GO@COF/GCE	DPV	0.5–200 μM	0.16	[37]
MWCNT-MIP-GCE	DPV	4–50 μM	0.68	[46]
Bismuth film-GCE	DPV	3.2–20.0 μM and 20.0–97.0 μM	2.1and12.2	[82]
Boron doped diamond electrode	SWV	8.01–119 μM	2.19	[49]
MoS_2-RuS_2/GCE	CV &Amperometry	0.01 to 598.7 μM	0.004	[83]
$ZnMn_2O_4$-GCE	DPV	0.008–1264 μM	0.0021	[84]
P3MT	SWV	5.0–3200 μM	4	[60]
CNPE	SWV	1–75 μM	0.4	[61]
GCE	LWV/DPV	15 −60 μM	5.4/8.5	[85]
Cu_2Sb/SPCE	DPV	0.09–818.18 μM	0.07	[86]
$MnCo_2O_4$/P-doped g-C_3N_4/GCE	CV, amperometry, DPV	0.008–207.57 and 0.01–95.40 μM	1.2 and 3 nM	[66]
CuNPs/MIP-OPPy/GCE	DPV	0.001 −10 μM	3.1×10^{-1} ° M	[76]
MIP@$CuInS_2$/ZnS/GCE	DPV/ratiometric mode	NA	2.1 nM	[77]
Nb_2CTx/AgNWs-MIP/GCE	CV	0.01–100 μM	1.30 nM	[78]
SDZ-MIP/APTES-ITO	CV/DPV	0.1–300 μM	0.11 μM	[79]
CNFs@Sb_2O_3/GCE	CV	0.083–24 μM	9.5×10^{-1} ° M	[80]
SnO_2-PANI/MCPE	DPV	40 μM to 280 μM	75.6	Present work

*NA: Not Available

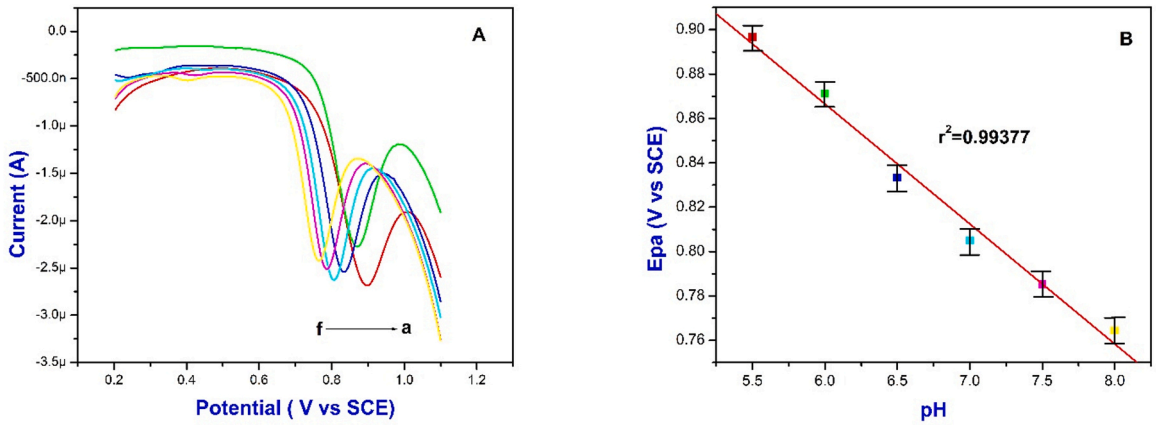

Fig. 8. **(A)** Cyclic voltammograms of SDZINE at MCPE in 0.2 M PBS across various pH levels from 5.5 to 8.0 at a scan rate of 0.05 V/s. **(B)** Calibration plot of anodic peak potential Epa versus pH.

approximately 54 mV/pH (Eq. 6), which is close to the theoretical Nernstian value of 59 mV/pH at 25°C. This suggests that the oxidation process involves an approximately equal number of electrons and protons. Therefore, the SDZINE oxidation mechanism at SnO_2-PANI/MCPE can be interpreted as a proton-coupled electron-transfer process, consistent with the proposed electro-oxidation pathway. The anodic peak current was found to vary with pH, reaching a maximum at pH 7.5. Hence, pH 7.4 was selected as the optimal working condition, as it closely resembles the physiological pH of human blood, tissues, and extracellular fluids.

$$E_{pa}\ (V) = -0.0541pH + 1.1912 \quad (6)$$

These experimental results were in good agreement with the previous report [88].

3.9. Interference study

To assess the selectivity of the SnO_2-PANI/MCPE sensor, interference studies were conducted under optimal experimental conditions. The impact of various potentially interfering species commonly present in pharmaceutical or biological matrices was evaluated by adding 1.0 mM solutions of ammonium chloride, gallic acid, potassium chloride, folic acid, urea, starch, glucose, magnesium chloride, calcium chloride, and zinc nitrate to the 0.1 mM SDZINE solution at pH 7.4. The results indicated that these substances did not produce any significant change in the oxidation peak current or potential of SDZINE. The variations in E_{pa} remained within ±5%, confirming negligible interference from these ions and molecules (Table 4). The negligible interference observed for the tested species can be explained by their electrochemical behavior under the selected experimental conditions. Inorganic ions such as NH_4^+, K^+, Mg^{2+}, Ca^{2+}, and $Zn^{2+}$are not expected to undergo significant oxidation within the potential window used for SDZINE detection and therefore do not produce overlapping anodic responses. In addition, the supporting phosphate buffer at pH 7.4 maintains a stable ionic environment, reducing changes in migration current and solution conductivity. Neutral organic species such as glucose, urea, and starch also showed negligible effect, probably because they are poorly oxidized at the SDZINE oxidation potential and do not strongly compete with SDZINE for active sites on the SnO_2–PANI/MCPE surface. Although gallic acid can be electroactive under certain conditions,it's presence did not significantly alter the SDZINE peak response in the present system, suggesting limited overlap with the SDZINE oxidation signal or weak competitive interaction with the modified electrode surface. Therefore, the observed selectivity may be attributed to the combined effect of the selected working potential, buffer conditions, and the favorable interaction of SDZINE with the SnO_2-PANI/MCPE. These findings demonstrate the high selectivity of the developed sensor for SDZINE detection, even in the presence of common interfering substances.

Tablee.4
Study of interference ions on SDZINE.

Interferents	Concentration (mM)	Epa	Signal change (%) (ΔEpa)
Gallic Acid	1.0	0.8058	1.37
Calcium Chloride	1.0	0.7923	0.3
Potassium Chloride	1.0	0.7923	0.3
Magnesium Chloride	1.0	0.7907	0.5
Ammonium Chloride	1.0	0.7907	0.5
Zinc Nitrate	1.0	0.7916	0.3
Starch	1.0	0.7916	0.3
Glucose	1.0	0.7916	0.3

3.10. Reproducibility, stability and repeatability

The stability, repeatability, and reproducibility of SnO_2-PANI/MCPE were evaluated for SDZINE determination. Short term stability was assessed over 15 days by recording the anodic peak current every 3 days under identical conditions, showing only minor variation with an RSD of 9.58% (Fig. 9A). Repeatability was evaluated through five successive SDZINE measurements using the same electrode, giving an RSD of 5.09% (Fig. 9B). Reproducibility was assessed using five independently prepared SnO_2-PANI/MCPEs, with an RSD of 3.10% (Figs. 9C, 9D). These results indicate acceptable stability, good repeatability, and satisfactory reproducibility of the fabricated sensor for SDZINE detection.

3.11. SDZINE determination in real sample

To evaluate the practical applicability of the developed SnO_2-PANI/MCPE for SDZINE detection, the sensor was applied to a real sample matrix, commercial cow milk. The experiment was designed to assess both detection capability and recovery performance in a complex biological sample. The detailed procedure of milk sample preparation is given in Section 2.5.

The recovery percentages of the spiked milk solutions were found to be in the range of 95.6–97.5% indicating excellent accuracy and minimal matrix interference from the milk sample (Table 5). The consistent increase in peak current with increasing SDZ concentration, along with stable peak potentials, confirms the sensor's selectivity and sensitivity in a real-world biological matrix. These results validate the use of the SnO_2-PANI/MCPE sensor as a reliable and sensitive platform for detecting SDZINE in complex food samples such as milk, with minimal sample pretreatment and high recovery efficiency.

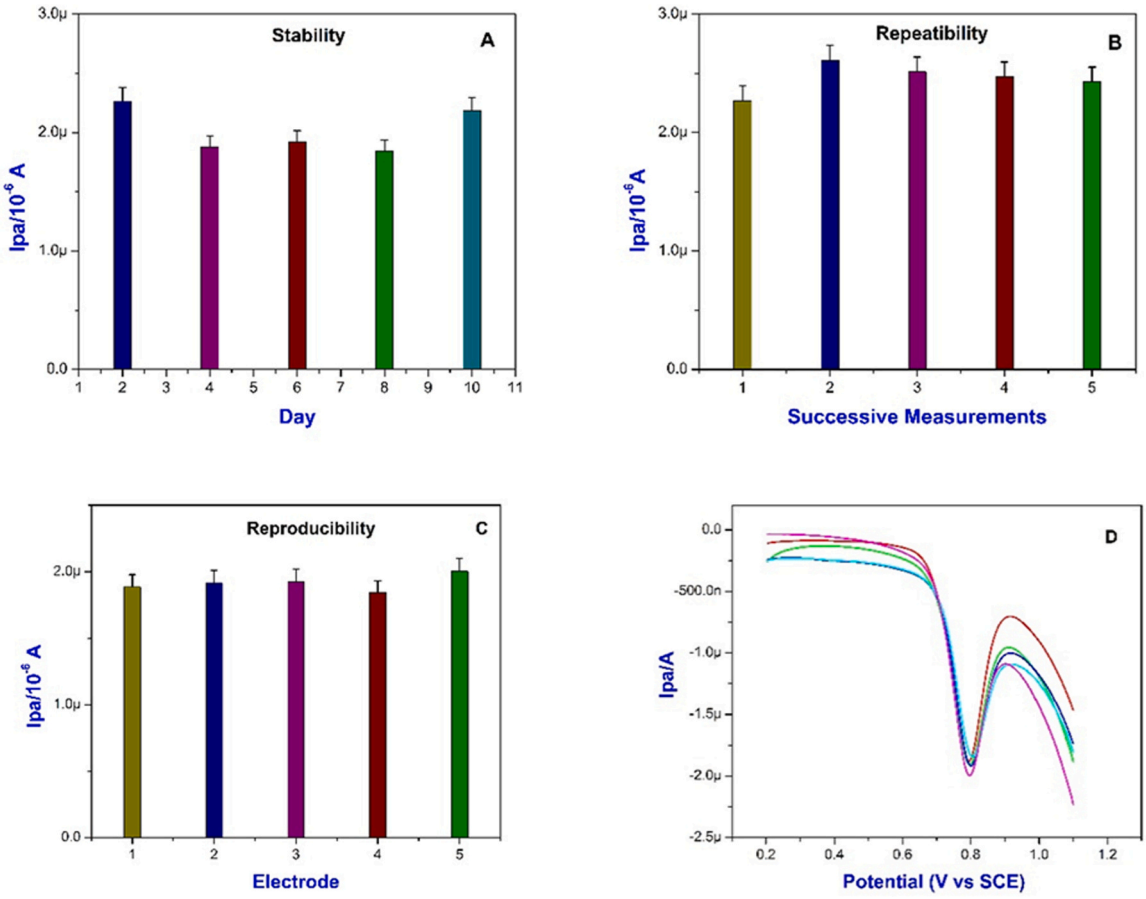

Fig. 9. Performance evaluation of the SnO_2–PANI/MCPE sensor for SDZINE detection: (A) stability response recorded over 15 days, (B) repeatability response obtained from five successive measurements using the same electrode, (C) reproducibility response obtained from five independently fabricated electrodes, and (D) corresponding DPV curves recorded using five separately prepared SnO_2-PANI/MCPEs.

Table 5
Recovery results for SDZINE in spiked milk samples.

Spiked SDZ (μM)	Detected SDZ (μM)	Recovery (%)	Epa (V)	Ipa (μA)
50	47.8	95.6	0.873	–1.48
100	97.2	97.2	0.880	–1.91
150	143.9	95.9	0.896	–2.22
200	195.1	97.5	0.899	–2.64

4. .0. Conclusion

In this study, a SnO_2–PANI nanocomposite-modified carbon paste electrode (SnO2-PANI/MCPE) was successfully fabricated and evaluated as an electrochemical sensing platform for SDZINE detection. SEM-EDX, XRD, and FTIR analyses supported the formation of the SnO_2-PANI-modified electrode, while electrochemical studies confirmed improved anodic response toward SDZINE oxidation. Compared with BCPE, SnO_2-MCPE, and PANI-MCPE, the SnO_2-PANI/MCPE showed the highest anodic peak current, supporting the synergistic contribution of SnO_2 surface-active catalytic sites and PANI conductive pathways.

The sensor showed a linear DPV response over 40–280 μM, with a sensitivity of 0.019639 μA μM^{-1}, an area-normalized sensitivity of 1.29 μA μM^{-1} cm^{-2}, an LOD of 75.72 μM, and an LOQ of 252.41 μM. Although this detection limit is not lower than several advanced reported SDZINE sensors, the present platform offers advantages of simple fabrication, low-cost materials, acceptable analytical performance, and practical usability. Scan-rate and pH studies suggested that SDZINE oxidation at the SnO_2-PANI/MCPE surface follows a mixed diffusion-adsorption controlled and proton-involved electrochemical process. The sensor also demonstrated good anti-interference performance against common matrix components, acceptable short-term stability over 15 days, good repeatability, and satisfactory reproducibility using independently fabricated electrodes.

The applicability of the method was demonstrated in spiked milk samples, where recoveries of 95.6–97.5% were obtained. Therefore, the SnO_2–PANI/MCPE can be considered a proof-of-concept electrochemical sensing platform for SDZINE determination in milk matrices. Future work should focus on improving the detection limit through optimization of the SnO_2:PANI ratio, modifier loading, film thickness, and signal-to-noise response. Validation at lower concentration ranges, incorporation of preconcentration strategies, testing with naturally contaminated or certified reference samples, and additional characterization using EIS, XPS, Raman, TEM, and BET analysis would further strengthen the analytical and mechanistic applicability of this sensor for residue-level food-safety monitoring.

5. .0. Future scope

Although the SnO_2–PANI/MCPE demonstrated acceptable sensitivity for SDZINE detection, the detection limit could potentially be further reduced through additional electrode and method optimization. Since LOD depends on the relationship between background noise and analytical sensitivity, future improvements should focus on increasing the calibration slope and minimizing baseline noise. This may be achieved by optimizing the SnO_2:PANI ratio, controlling nanocomposite particle size and film thickness, improving dispersion uniformity, and increasing the electroactive surface area without blocking electron

transfer. Incorporation of highly conductive carbon nanomaterials such as graphene, reduced graphene oxide, or carbon nanotubes may further improve charge-transfer kinetics and signal amplification. In addition, molecularly imprinted or affinity-based surface layers could improve SDZINE preconcentration and selectivity at the electrode interface. Optimization of pulse voltammetric parameters, accumulation time, accumulation potential, and sample pretreatment may also reduce matrix-related noise and improve the signal-to-noise ratio in milk samples. These strategies will be explored in future studies to improve trace-level SDZINE detection.

CRediT authorship contribution statement

Ramesh S. Malladi: Writing – review & editing, Visualization, Validation, Supervision, Software, Methodology, Investigation, Funding acquisition, Formal analysis, Data curation. **Kailash S. Chadchan:** Writing – review & editing, Visualization, Validation, Software, Resources, Methodology, Investigation, Formal analysis, Data curation. **N. Das Swastika:** Writing – review & editing, Writing – original draft, Visualization, Validation, Supervision, Software, Resources, Project administration, Methodology, Investigation, Formal analysis, Data curation, Conceptualization. **Aishwarya S. Sajjan:** Writing – review & editing, Writing – original draft, Visualization, Validation, Software, Methodology, Investigation, Formal analysis, Data curation.

Declaration of Competing Interest

The authors declare that they have no known competing financial interests or personal relationships that could have appeared to influence the work reported in this paper.

Acknowledgements

We wish to express our gratitude to VGST (Vision Group of Science and Technology), Karnataka Science and Technology Promotion Society, Government of Karnataka, India, for funding the work. [Ref. No: VGST/RGS-F/GRD No. 888/2019–20/2020–2021/198].

We are thankful to Dr. Sayandeep K. Das for preparing the graphical abstract and helping in technical work.

Appendix A. Supporting information

Supplementary data associated with this article can be found in the online version at doi:10.1016/j.nxmate.2026.102399.

References

[1] A.M. Brezoiu, M. Deaconu, I. Nicu, E. Vasile, R.A. Mitran, C. Matei, et al., Heteroatom modified MCM-41-silica carriers for Lomefloxacin delivery systems, Microporous Mesoporous Mater. 275 (2019) 214–222, https://doi.org/10.1016/J.MICROMESO.2018.08.031.

[2] T. Yadavalli, D. Shukla, Role of metal and metal oxide nanoparticles as diagnostic and therapeutic tools for highly prevalent viral infections, Nanomedicine 13 (2017) 219–230, https://doi.org/10.1016/J.NANO.2016.08.016.

[3] R.C. Mundargi, V.R. Babu, V. Rangaswamy, P. Patel, T.M. Aminabhavi, Nano/micro technologies for delivering macromolecular therapeutics using poly(d,l-lactide-co-glycolide) and its derivatives, J. Control. Release 125 (2008) 193–209, https://doi.org/10.1016/J.JCONREL.2007.09.013.

[4] S.Y. Won, C.H. Lee, H.S. Chang, S.O. Kim, S.H. Lee, D.S. Kim, Monitoring of 14 sulfonamide antibiotic residues in marine products using HPLC-PDA and LC-MS/MS, Food Control. 22 (7) (2011) 1101, https://doi.org/10.1016/J.FOODCONT.2011.01.005.

[5] T. Yadavalli, S. Ramasamy, G. Chandrasekaran, I. Michael, H.A. Therese, R. Chennakesavulu, Dual responsive PNIPAM–chitosan targeted magnetic nanopolymers for targeted drug delivery, J. Magn. Magn. Mater. 380 (2015) 315–320, https://doi.org/10.1016/J.JMMM.2014.09.035.

[6] J.C. Goloboy, W.G. Klemperer, T.A. Marquart, G. Westwood, O.M. Yaghi, Complex Oxides as Molecular Materials: Structure and Bonding in High-Valent Early Transition Metal Compounds. Polyoxometalate Molecular Science, Springer Netherlands, Dordrecht, 2003, pp. 79–174, https://doi.org/10.1007/978-94-010-0091-8_4.

[7] L. He, Y. Su, J. Lanhong, S. Shi, Recent advances of cerium oxide nanoparticles in synthesis, luminescence and biomedical studies: a review, J. Rare Earths 33 (2015) 791–799, https://doi.org/10.1016/S1002-0721(14)60486-5.

[8] M.R. Mahmoudian, W.J. Basirun, M. Sookhakian, P.M. Woi, E. Zalnezhad, H. Hazarkhani, et al., Synthesis and characterization of α-Fe2O3/polyaniline nanotube composite as electrochemical sensor for uric acid detection, Adv. Powder Technol. 30 (2019) 384–392, https://doi.org/10.1016/j.apt.2018.11.015.

[9] B. Muthukutty, J. Ganesamurthi, S.-M. Chen, B. Arumugam, F. mao chang, S. M. Wabaidur, et al., Construction of novel binary metal oxides: copper oxide–tin oxide nanoparticles regulated for selective and nanomolar level electrochemical detection of anti-psychotic drug, Electrochim. Acta 386 (2021) 138482, https://doi.org/10.1016/j.electacta.2021.138482.

[10] T.P. Tsele, A.S. Adekunle, O.E. Fayemi, E.E. Ebenso, Electrochemical detection of Epinephrine using Polyaniline nanocomposite films doped with TiO2 and RuO2 nanoparticles on multi-walled carbon nanotube, Electrochim. Acta 243 (2017) 331–348, https://doi.org/10.1016/J.ELECTACTA.2017.05.031.

[11] P. Niu, M. Gich, A. Roig, C. Fernández-Sánchez, Metal nanoparticle carbon gel composites in environmental water sensing applications, Chem. Rec. 18 (2018) 749–758, https://doi.org/10.1002/tcr.201800011.

[12] M. Chen, Y. Cui, W. Qian, Q. Peng, J. Wang, H. Gong, et al., Thermoregulated ionic liquid-stabilizing Ru/CoO nanocomposites for catalytic hydrogenation, Langmuir 36 (2020) 11589–11599, https://doi.org/10.1021/acs.langmuir.0c02153.

[13] M.R. Ganjali, H. Salimi, S. Tajik, H. Beitollahi, M. Rezapour, B. Larijani, Application of Fe3O4@SiO2/MWCNT Film on glassy carbon electrode for the sensitive electroanalysis of Levodopa, Int. J. Electrochem. Sci. 12 (2017) 5243–5253, https://doi.org/10.20964/2017.06.88.

[14] M.S. Abdelrahman, S.H. Nassar, H. Mashaly, S. Mahmoud, D. Maamoun, M. El-Sakhawy, et al., Studies of polylactic acid and metal oxide nanoparticles-based composites for multifunctional textile prints, Coatings 10 (2020) 58, https://doi.org/10.3390/coatings10010058.

[15] A. Kumar, L. Rout, R.S. Dhaka, S.L. Samal, P. Dash, Design of a graphene oxide-SnO_2 nanocomposite with superior catalytic efficiency for the synthesis of β-enaminones and β-enaminoesters, RSC Adv. 5 (2015) 39193–39204, https://doi.org/10.1039/C5RA03363B.

[16] M. Rumyantseva, V. Kovalenko, A. Gaskov, E. Makshina, V. Yuschenko, I. Ivanova, et al., Nanocomposites SnO2/Fe2O3: sensor and catalytic properties, Sens. Actuators B Chem. 118 (2006) 208–214, https://doi.org/10.1016/j.snb.2006.04.024.

[17] P. Veerakumar, C. Koventhan, S.M. Chen, Copper-palladium alloy nanoparticles immobilized over porous carbon for voltammetric determination of dimetridazole, J. Alloy. Compd. 931 (2023) 167474, https://doi.org/10.1016/J.JALLCOM.2022.167474.

[18] R. Pandiyan, V. Vinothkumar, S.M. Chen, P. Veerakumar, T.H. Kim, Polyol-assisted synthesis of NdFeO3 nanoparticles decorated porous N-CNTs for voltammetric sensing of furazolidone in veterinary feeds and urine samples, Surf. Interfaces 49 (2024) 104365, https://doi.org/10.1016/J.SURFIN.2024.104365.

[19] R. Pandiyan, P. Veerakumar, S.M. Chen, J.T. Liu, Hydrothermal synthesis of DyNbO4 hallow spheres anchored on heteroatoms-doped reduced graphene oxide for electrochemical detection of environmental pollutant 4-nitrotoluene, J. Environ. Chem. Eng. 13 (2025) 116450, https://doi.org/10.1016/J.JECE.2025.116450.

[20] S. Kulkarni, P. Patil, A. Mujumdar, J. Naik, Synthesis and evaluation of gas sensing properties of PANI, PANI/SnO2 and PANI/SnO2/rGO nanocomposites at room temperature, Inorg. Chem. Commun. 96 (2018) 90–96, https://doi.org/10.1016/J.INOCHE.2018.08.008.

[21] A.M. Sudapalli, N.G. Shimpi, Tetragonal SnO2 nanoparticles: an efficient photocatalyst for the degradation of hazardous ionic dyes, ChemistrySelect 8 (2023) e202203310, https://doi.org/10.1002/SLCT.202203310;WGROUP:STRING:PUBLICATION.

[22] M. Rahman, Tin oxide thin films for the future: a paradigm shift in property engineering for advanced functional devices, Materials 9 (2025) 101341, https://doi.org/10.1016/j.nxmate.2025.101341.

[23] N. Wang, Y. Du, W. Ma, P. Xu, X. Han, Rational design and synthesis of SnO2-encapsulated α-Fe2O3 nanocubes as a robust and stable photo-Fenton catalyst, Appl. Catal. B 210 (2017) 23–33, https://doi.org/10.1016/j.apcatb.2017.03.037.

[24] A. Majid, J. Tunney, S. Argue, D. Kingston, M. Post, J. Margeson, et al., Characterization of CuO phase in SnO2–CuO prepared by the modified Pechini method, J. Solgel Sci. Technol. 53 (2010) 390–398, https://doi.org/10.1007/s10971-009-2108-x.

[25] M. Rajesh Kumar, G. Murugadoss, A.N. Pirogov, R. Thangamuthu, A facile one step synthesis of SnO2/CuO and CuO/SnO2 nanocomposites: photocatalytic application, Journal Materials Science Materials Electronics 29 (2018) 13508–13515, https://doi.org/10.1007/s10854-018-9476-3.

[26] H.M. Aliha, A.A. Khodadadi, Y. Mortazavi, The sensing behaviour of metal oxides (ZnO, CuO and Sm2O3) doped-SnO2 for detection of low concentrations of chlorinated volatile organic compounds, Sens. Actuators B Chem. 181 (2013) 637–643, https://doi.org/10.1016/J.SNB.2013.02.055.

[27] Y. Wang, X. Hu, K. Zheng, X. Wei, Y. Zhao, Effect of SnO2 on the structure and catalytic performance of Co3O4 for N2O decomposition, Catal. Commun. 111 (2018) 70–74, https://doi.org/10.1016/j.catcom.2018.04.004.

[28] B. Faniband, S.S. Chandra, A. Hiremath, J. Pattar, R. Sreekanth, K. Mahendra, et al., Enhanced charge transport and interfacial polarization in PANI/SnO2 nanocomposites, Materials Science Engineering B 323 (2026) 118792, https://doi.org/10.1016/J.MSEB.2025.118792.

[29] S. Singh, N. Verma, A. Singh, B.C. Yadav, Synthesis and characterization of CuO–SnO2 nanocomposite and its application as liquefied petroleum gas sensor,

Mater. Sci. Semicond. Process. 18 (2014) 88–96, https://doi.org/10.1016/J.MSSP.2013.11.002.
[30] P.G. Shetty, A.M. Sudapalli, Investigating the synergistic effect of CuO and PANI-CuO composite for high-performance supercapacitor studies, Materials 9 (2025) 101287, https://doi.org/10.1016/j.nxmate.2025.101287.
[31] N. Aydemir, J. Malmström, J. Travas-Sejdic, Conducting polymer based electrochemical biosensors, Phys. Chem. Chem. Phys. 18 (2016) 8264–8277, https://doi.org/10.1039/C5CP06830D.
[32] Y.-Z. Long, M.-M. Li, C. Gu, M. Wan, J.-L. Duvail, Z. Liu, et al., Recent advances in synthesis, physical properties and applications of conducting polymer nanotubes and nanofibers, Prog. Polym. Sci. 36 (2011) 1415–1442, https://doi.org/10.1016/j.progpolymsci.2011.04.001.
[33] M.H. Naveen, N.G. Gurudatt, Y.-B. Shim, Applications of conducting polymer composites to electrochemical sensors: a review, Appl. Mater. Today 9 (2017) 419–433, https://doi.org/10.1016/j.apmt.2017.09.001.
[34] O.E. Fayemi, A.S. Adekunle, B.E. Kumara Swamy, E.E. Ebenso, Electrochemical sensor for the detection of dopamine in real samples using polyaniline/NiO, ZnO, and Fe3O4 nanocomposites on glassy carbon electrode, J. Electroanal. Chem. 818 (2018) 236–249, https://doi.org/10.1016/j.jelechem.2018.02.027.
[35] G. Stando, P. Stando, M. Sahlman, M. Lundström, H. Liu, D. Janas, Synthesis of nanocomposites via electropolymerization of aniline onto hydrophilic films from nanocarbon and investigation of their properties, Electrochim. Acta 463 (2023) 142842, https://doi.org/10.1016/J.ELECTACTA.2023.142842.
[36] S.S. Patil, K.V. Harpale, S.P. Koiry, K.R. Patil, D.K. Aswal, M.A. More, Multifunctional polyaniline–tin oxide (PANI–SnO $_2$) nanocomposite: synthesis, electrochemical, and field emission investigations, J. Appl. Polym. Sci. 132 (2015), https://doi.org/10.1002/app.41401.
[37] Y. Sun, J. He, G.I.N. Waterhouse, L. Xu, H. Zhang, X. Qiao, et al., A selective molecularly imprinted electrochemical sensor with GO@COF signal amplification for the simultaneous determination of sulfadiazine and acetaminophen, Sens. Actuators B Chem. 300 (2019) 126993, https://doi.org/10.1016/J.SNB.2019.126993.
[38] H. Ma, C. Li, J. Yin, X. Pu, D. Zhang, C. Su, et al., Polyoxometalate enhances the photocatalytic performance of polyaniline/SnO2 composites, Mater. Lett. 168 (2016) 103–106, https://doi.org/10.1016/J.MATLET.2016.01.041.
[39] H.C. Pant, M.K. Patra, S.C. Negi, A. Bhatia, S.R. Vadera, N. Kumar, Studies on conductivity and dielectric properties of polyaniline-zinc sulphide composites, Bull. Mater. Sci. 29 (2006) 379–384, https://doi.org/10.1007/BF02704139.
[40] R. Anitha, E. Kumar, K. Rathnakumar, S.C. Vella Durai, Synthesis, structural, morphological, optical and electrical studies of PANI/SnO_2 nanocomposites, J. Ovonic Res. 17 (2) (2021) 99–106, https://doi.org/10.15251/JOR.2021.172.99.
[41] G.Y. Zhao, H.L. Li, Preparation of polyaniline nanowire arrayed electrodes for electrochemical supercapacitors, Microporous Mesoporous Mater. 110 (2008) 590–594, https://doi.org/10.1016/J.MICROMESO.2007.06.023.
[42] S. Kumar, R.B. Choudhary, Structural, optical, and thermal investigation of SnO_2 nanoparticles incorporated PANI nanofibers as an emissive layer material, J. Mol. Struct. 1293 (2023) 136199, https://doi.org/10.1016/j.molstruc.2023.136199.
[43] V. Mozafari, J. Basiri Parsa, Electrochemical synthesis of Pd supported on PANI-MWCNTs-SnO_2 nanocomposite as a novel catalyst towards ethanol oxidation in alkaline media, Synth. Met. 259 (2020) 116214, https://doi.org/10.1016/J.SYNTHMET.2019.116214.
[44] H.M. Aliha, A.A. Khodadadi, Y. Mortazavi, M.N. Lotfollahi, Novel SnO_2/PANI nanocomposites for selective detection of ammonia at room temperature, Appl. Surf. Sci. 615 (2023) 156381, https://doi.org/10.1016/J.APSUSC.2023.156381.
[45] Z. Zhang, S. Zhai, M. Wang, L. He, D. Peng, S. Liu, et al., Electrochemical sensor based on a polyaniline-modified SnO $_2$ nanocomposite for detecting ethephon, Anal. Methods 7 (2015) 4725–4733, https://doi.org/10.1039/C5AY01028D.
[46] B. Liu, Y. Ma, F. Zhou, Q. Wang, G. Liu, Voltammetric determination of sulfadiazine based on molecular imprinted electrochemical sensor, Int. J. Electrochem. Sci. 15 (2020) 9590–9596, https://doi.org/10.20964/2020.10.10.
[47] M. Barfield, N. Spooner, R. Lad, S. Parry, S. Fowles, Application of dried blood spots combined with HPLC-MS/MS for the quantification of acetaminophen in toxicokinetic studies, J. Chromatogr. B 870 (2008) 32–37, https://doi.org/10.1016/J.JCHROMB.2008.05.025.
[48] M.J. García-Galán, M. Silvia Díaz-Cruz, D. Barceló, Identification and determination of metabolites and degradation products of sulfonamide antibiotics, TrAC. Trends Anal. Chem. 27 (2008) 1008–1022, https://doi.org/10.1016/j.trac.2008.10.001.
[49] C.D. Souza, O.C. Braga, I.C. Vieira, A. Spinelli, Electroanalytical determination of sulfadiazine and sulfamethoxazole in pharmaceuticals using a boron-doped diamond electrode, Sens. Actuators B Chem. 135 (2008) 66–73, https://doi.org/10.1016/J.SNB.2008.07.020.
[50] A.B. Teradale, S.N. Unki, P.S. Ganesh, K.K. Das, S.N. Das, Development of a diethylcarbamazine citrate-based electrochemical sensor for quick and affordable detection of sulfadiazine and uric acid in environmental monitoring, ChemistrySelect 9 (2024), https://doi.org/10.1002/slct.202401047.
[51] M.M. Fahad, M.G.A. Alkhuzaie, S.F. Ali, Recent advances in sulfadiazine's preparation, reactions and biological applications, Eurasian Chemical Communications 3 (6) (2021) 383–391.
[52] S. Sadeghi, A. Motaharian, Voltammetric sensor based on carbon paste electrode modified with molecular imprinted polymer for determination of sulfadiazine in milk and human serum, Mater. Sci. Eng. C 33 (2013) 4884–4891, https://doi.org/10.1016/J.MSEC.2013.08.001.
[53] Stephany, RainerW. The EU system of reference laboratories for residues in food of animal origin, Accrédit. Qual. Assur. 9 (2004), https://doi.org/10.1007/s00769-004-0823-0.
[54] A.R. Long, C.R. Short, S.A. Barker, Method for the isolation and liquid chromatographic determination of eight sulfonamides in milk, J. Chromatogr. A 502 (1990) 87–94, https://doi.org/10.1016/S0021-9673(01)89566-2.
[55] A.K. Vivekanandan, B. Muthukutty, S.M. Chen, M. Sivakumar, S.H. Chen, Intermetallic compound Cu_2Sb nanoparticles for effective electrocatalytic oxidation of an antibiotic drug: sulphadiazine, ACS Sustain. Chem. Eng. 8 (2020) 17718–17726, https://doi.org/10.1021/acssuschemeng.0c05629.
[56] B. Sriram, J.N. Baby, Y.-F. Hsu, S.-F. Wang, X. Benadict Joseph, M. George, et al., $MnCo_2O_4$ microflowers anchored on P-doped g -C $_3$ N $_4$ nanosheets as an electrocatalyst for voltammetric determination of the antibiotic drug sulfadiazine, ACS Appl. Electron. Mater. 3 (2021) 3915–3926, https://doi.org/10.1021/acsaelm.1c00506.
[57] S.P. Jacobsson, M. Carlsson, U. Jönsson, G. Nilsson, Quantitative determination of sulfasalazine by near-infrared spectroscopy and multivariate analysis in reflectance mode with a fibre-optic probe, J. Pharm. Biomed. Anal. 13 (1995) 415–417, https://doi.org/10.1016/0731-7085(95)01304-4.
[58] N. Arroyo-Manzanares, L. Gámiz-Gracia, A.M. García-Campaña, Alternative sample treatments for the determination of sulfonamides in milk by HPLC with fluorescence detection, Food Chem. 143 (2014) 459–464, https://doi.org/10.1016/J.FOODCHEM.2013.08.008.
[59] Z. Malá, P. Gebauer, P. Boček, New methodology for capillary electrophoresis with ESI-MS detection: electrophoretic focusing on inverse electromigration dispersion gradient. High-sensitivity analysis of sulfonamides in waters, Anal. Chim. Acta 935 (2016) 249–257, https://doi.org/10.1016/J.ACA.2016.06.016.
[60] T.A.M. Msagati, Ngila JC. Voltammetric detection of sulfonamides at a poly(3-methylthiophene) electrode, Talanta 58 (2002) 605–610, https://doi.org/10.1016/S0039-9140(02)00327-2.
[61] A. Ait Lahcen, S. Ait Errayess, A. Amine, Voltammetric determination of sulfonamides using paste electrodes based on various carbon nanomaterials, Microchim. Acta 183 (2016) 2169–2176, https://doi.org/10.1007/s00604-016-1850-3.
[62] G. Kudur Jayaprakash, B.E.K. Swamy, R. Flores-Moreno, K. Pineda-Urbina, Theoretical and cyclic voltammetric analysis of asparagine and glutamine electrocatalytic activities for dopamine sensing applications, Catalysts 13 (2023) 100, https://doi.org/10.3390/CATAL13010100.
[63] G. Kudur Jayaprakash, B.E.K. Swamy, N. Casillas, R. Flores-Moreno, Analytical Fukui and cyclic voltammetric studies on ferrocene modified carbon electrodes and effect of Triton X-100 by immobilization method, Electrochim. Acta 258 (2017) 1025–1034, https://doi.org/10.1016/J.ELECTACTA.2017.11.154.
[64] O.C. Braga, I. Campestrini, I.C. Vieira, A. Spinelli, Sulfadiazine determination in pharmaceuticals by electrochemical reduction on a glassy carbon electrode, J. Braz. Chem. Soc. 21 (2010) 813–820, https://doi.org/10.1590/S0103-50532010000500008.
[65] I.J.D. Priscillal, A.A. Alothman, S.-F. Wang, R. Arumugam, Lanthanide type of cerium sulfide embedded carbon nitride composite modified electrode for potential electrochemical detection of sulfaguanidine, Microchim. Acta 188 (2021) 313, https://doi.org/10.1007/s00604-021-04975-y.
[66] B. Sriram, J.N. Baby, Y.F. Hsu, S.F. Wang, X. Benadict Joseph, M. George, et al., $MnCo_2O_4$ Microflowers anchored on P-Doped g-C_3N4 nanosheets as an electrocatalyst for voltammetric determination of the antibiotic drug sulfadiazine, ACS Appl. Electron. Mater. 3 (2021) 3915–3926, https://doi.org/10.1021/ACSAELM.1C00506.
[67] N. Shahzad, N. Ali, A. Shahid, S. Khan, H. Alrobei, Synthesis of tin oxide nanoparticles in order to study its properties, Dig. J. Nanomater. Biostruct. 16 (1) (2021) 41–49, https://doi.org/10.15251/DJNB.2021.161.41.
[68] K.S. Chadchan, B.M. Basha, A.B. Teradale, S.N. Das, Electrochemical study of tartrazine on a diethylcarbamazine modified carbon paste electrode surface for enhancing food safety, Chem. Pap. 79 (2025) 8455–8466, https://doi.org/10.1007/s11696-025-04325-9.
[69] A.B. Teradale, S.D. Lamani, P.S. Ganesh, B.E. Kumara Swamy, S.N. Das, CTAB immobilized carbon paste electrode for the determination of mesalazine: a cyclic voltammetric method, Sens. Biosens. Res. 15 (2017) 53–59, https://doi.org/10.1016/j.sbsr.2017.08.001.
[70] S. Haq, P. Ahmad, M.U. Khandaker, M.R.I. Faruque, W. Rehman, M. Waseem, et al., Antibacterial, antioxidant and physicochemical investigations of tin dioxide nanoparticles synthesized via microemulsion method, Mater. Res. Express 8 (2021) 035013, https://doi.org/10.1088/2053-1591/abed8a.
[71] S. Tazikeh, A. Akbari, A. Talebi, E. Talebi, Synthesis and characterization of tin oxide nanoparticles via the Co-precipitation method, Mater. Sci. -Pol. 32 (1) (2014) 98–101, https://doi.org/10.2478/s13536-013-0164-y.
[72] Z.A. Hu, Y.L. Xie, Y.X. Wang, L.P. Mo, Y.Y. Yang, Z.Y. Zhang, Polyaniline/SnO_2 nanocomposite for supercapacitor applications, Mater. Chem. Phys. 114 (2009) 990–995, https://doi.org/10.1016/J.MATCHEMPHYS.2008.11.005.
[73] N.G. Deshpande, Y.G. Gudage, R. Sharma, J.C. Vyas, J.B. Kim, Y.P. Lee, Studies on tin oxide-intercalated polyaniline nanocomposite for ammonia gas sensing applications, Sens. Actuators B Chem. 138 (2009) 76–84, https://doi.org/10.1016/J.SNB.2009.02.012.
[74] S.B. Arpitha, B.E.K. Swamy, ZnO/poly(nigrosine)/modified carbon paste electrode for selective sensing of vanillin in the presence of amaranth: a voltammetric study, 2024;62, J. Food Sci. Technol. 62 (6) (2024) 1057–1064, https://doi.org/10.1007/s13197-024-06122-w.
[75] Y. Zhou, W. Tang, J. Wang, G. Zhang, S. Chai, L. Zhang, et al., Selective determination of dopamine and uric acid using electrochemical sensor based on poly(alizarin yellow R) film-modified electrode, Anal. Methods 6 (2014) 3474–3481, https://doi.org/10.1039/C3AY42216J.

[76] M.B. Elamin, S.M.A. Ali, H. Essousi, A. Chrouda, L.M. Alhaidari, N. Jaffrezic-Renault, et al., An Electrochemical sensor for sulfadiazine determination based on a copper nanoparticles/molecularly imprinted overoxidized polypyrrole composite, Sensors 23 (2023) 1270, https://doi.org/10.3390/S23031270.
[77] X. Yu, Y. Yang, Q. Shen, Y. Sun, Q. Kang, D. Shen, A novel differential ratiometric molecularly imprinted electrochemical sensor for determination of sulfadiazine in food samples, 137461, Food Chem. 434 (2023) 137461, https://doi.org/10.1016/j.foodchem.2023.137461.
[78] Y. Wang, J. He, J. Wu, W. Hao, L. Cai, H. Wang, et al., A novel molecularly imprinted electrochemical sensor based on quasi-three-dimensional nanomaterials Nb_2CTx/AgNWs for specific detection of sulfadiazine, Microchim. Acta 191 (11) (2024) 720, https://doi.org/10.1007/S00604-024-06805-3.
[79] S. Chopra, M. Balkhandia, M. Khatak, N. Sagar, Ved Agrawal, V. Molecularly imprinted electrochemical sensor based on APTES-functionalized indium tin oxide electrode for the determination of sulfadiazine 191 (2024) 727, https://doi.org/10.1007/s00604-024-06781-8.
[80] E. Beyyavaş, M. Aslanoglu, A CNF–Sb_2O_3 nanostructured electrochemical platform for trace-level sulfadiazine sensing and monitoring, Microchem. J. 218 (2025) 115554, https://doi.org/10.1016/J.MICROC.2025.115554.
[81] L. Fotouhi, A.B. Hashkavayi, M.M. Heravi, Electrochemical behaviour and voltammetric determination of sulphadiazine using a multi-walled carbon nanotube composite film-glassy carbon electrode, J. Exp. Nanosci. 8 (2013) 947–956, https://doi.org/10.1080/17458080.2011.624554.
[82] I. Campestrini, O.C. de Braga, I.C. Vieira, A. Spinelli, Application of bismuth-film electrode for cathodic electroanalytical determination of sulfadiazine, Electrochim. Acta 55 (2010) 4970–4975, https://doi.org/10.1016/J.ELECTACTA.2010.03.105.
[83] R. Sakthivel, S. Kubendhiran, S.M. Chen, T.W. Chen, N. Al-Zaqri, A. Alsalme, et al., Exploring the promising potential of MoS_2–RuS_2 binary metal sulphide towards the electrocatalysis of antibiotic drug sulphadiazine, Anal. Chim. Acta 1086 (2019) 55–65, https://doi.org/10.1016/j.aca.2019.07.073.
[84] S. Vinoth, M. Govindasamy, S.-F. Wang, A.A. Alothman, R.A. Alshgari, Hydrothermally synthesized cubical zinc manganite nanostructure for electrocatalytic detection of sulfadiazine, Microchim. Acta 188 (2021) 131, https://doi.org/10.1007/s00604-021-04768-3.
[85] J.M. Pingarron Carrazon, P. Corona Corona, L.M. Polo Diez, Electroanalytical study of sulphadiazine at solid electrodes. Determination in pharmaceutical preparations, Electrochim. Acta 32 (1987) 1573–1575, https://doi.org/10.1016/0013-4686(87)90006-5.
[86] A.K. Vivekanandan, B. Muthukutty, S.M. Chen, M. Sivakumar, S.H. Chen, Intermetallic compound Cu_2Sb nanoparticles for effective electrocatalytic oxidation of an antibiotic drug: sulphadiazine, ACS Sustain. Chem. Eng. 8 (2020) 17718–17726, https://doi.org/10.1021/ACSSUSCHEMENG.0C05629.
[87] A.B. Teradale, K.S. Chadchan, P.-S. Ganesh, S.N. Das, E.E. Ebenso, Synergetic effects of a poly-tartrazine/CTAB modified carbon paste electrode sensor towards simultaneous and interference-free determination of benzenediol isomers, React. Chem. Eng. 8 (2023) 3071–3081, https://doi.org/10.1039/D3RE00318C.
[88] Solomon Mehretie SAMT, T.S. Voltammetric, Determination of paracetamol with Poly(3,4-Ethylenedioxythiophene) modified glassy carbon electrode. analytical & bioanalytical, Electrochemistry 3 (2011) 38–50.